Electrochimica Acta 308 (2019) 131–141

Contents lists available at ScienceDirect

Electrochimica Acta

journal homepage: www.elsevier.com/locate/electacta

Investigation on the polarization resistance of steel embedded in highly resistive cementitious systems – An attempt and challenges

Sripriya Rengaraju [a], Lakshman Neelakantan [b], Radhakrishna G. Pillai [a, *]

[a] Department of Civil Engineering, Indian Institute of Technology Madras, Chennai, India
[b] Corrosion Engineering & Materials Electrochemistry Laboratory, Department of Metallurgical Materials and Engineering, Indian Institute of Technology Madras, Chennai, India

ARTICLE INFO

Article history:
Received 8 January 2019
Received in revised form
12 March 2019
Accepted 28 March 2019
Available online 29 March 2019

Keywords:
Cement
Concrete
Steel
Corrosion
Durability
Electrochemical testing
Resistivity
Polarization resistance
Electrochemical impedance spectroscopy
Equivalent circuit

ABSTRACT

Concretes with fly ash, slag, limestone calcined clay, etc. exhibiting high resistivity are being used to enhance the chloride resistance of structures – to achieve durability. Prior to use, the engineers need to determine the chloride threshold (Cl_{th}) of such highly resistive steel cementitious (S-C) systems (a key parameter to estimate service life). Most Cl_{th} tests involve repeated measurements of polarization resistance (R_p) and detection of corrosion initiation of steel embedded in hardened cementitious system (a sol-gel structure with partially filled pores). The high resistivity of such systems should be considered while interpreting the electrochemical response to determine R_p. This paper experimentally evaluates the suitability of LPR and EIS techniques for assessing R_p of steel embedded in highly resistive systems. Experiments were conducted with lollipop type specimens (steel reinforcement embedded in mortar cylinders). The following three types of mortar having various resistivities were prepared: (i) ordinary portland cement (OPC), (ii) OPC + fly ash, and (iii) limestone calcined clay cement. Experimental observations on how the following three factors affect the electrochemical response in highly resistive S-C systems are provided: (i) resistivity of concrete covering the embedded steel, (ii) electrode configuration, and (iii) electrochemical test parameters. It was found that electrochemical impedance spectroscopy (EIS) can detect corrosion initiation in highly resistive systems at earlier stages than the linear polarization resistance (LPR) technique. Also, the guidelines on how to use EIS technique to determine the R_p of steel embedded in highly resistive S-C systems are provided.

1. Introduction

Many concrete structures made of ordinary portland cement (OPC) systems are experiencing premature corrosion due to exposure to chlorides. This led to the partial replacement of OPC with pulverized fuel ash (PFA), [PFA is also known as fly ash], which enhances the resistivity of concrete against the ingress of chlorides; thereby enhancing the service life of concrete structures. Recently, a new type of cement called limestone calcined clay cement (LC3) with very high electrical resistivity is also being developed [1,2]. Prior to the widespread use of any material, engineers need to assess its effect on the service life of reinforced concrete systems. One of the critical service life parameters for any steel-cementitious (S-C) system is the chloride threshold (Cl_{th}), which is defined as the minimum amount of chlorides required to initiate the corrosion of the embedded steel reinforcement. The assessment of Cl_{th} of S-C systems is highly dependent on the quality of the electrochemical response and its interpretation, which is the focus of this paper.

The electrochemical response from S-C systems depends on the (i) properties of cover concrete, (ii) properties of steel reinforcement, (iii) microclimate at the S-C interface, (iv) electrochemical technique adopted, and (v) corrosion cell (configuration of specimen and electrodes). In this paper, the major focus is on the effect of highly resistive concrete cover, which induces significant ohmic drop and influences the use of electrochemical measurement techniques. Assessment of this ohmic drop and its incorporation to get correct polarization resistance (R_p) of the steel embedded in cementitious system is very important. This becomes very challenging as the resistivity of concrete cover increases. The techniques which may work well for low resistive concretes may not work for highly resistive concretes. In this paper, the effectiveness of linear polarization resistance (LPR) and electrochemical

* Corresponding author.
E-mail address: pillai@iitm.ac.in (R.G. Pillai).

https://doi.org/10.1016/j.electacta.2019.03.200
0013-4686/

impedance spectroscopy (EIS) techniques in measuring R_p of steel embedded in low and highly resistive cementitious systems are evaluated.

1.1. Resistivity of concretes and corrosion mechanisms

Fig. 1 shows the range of surface resistivity exhibited by concretes made of OPC, PFA, and LC3 at 28 days of curing [2,3]. It has been observed that the resistivity of OPC systems cannot be more than say, 30 kΩ cm even if the water/binder is kept very low. Also, some of the PFA and all the LC3 concretes exhibit higher resistivity than all the OPC concretes. AASHTO T358 (2017) [4] recommends a classification for chloride resistance of concrete based on its surface resistivity, see Table 1. Following this, in general, the concretes with OPC, PFA, and LC3 can exhibit 'low to moderate', 'moderate to high' and 'very high' resistivities. It should be noted that in this paper, 'highly resistive' systems represent concretes with 'high' and 'very high' resistivities.

The electrochemical techniques adopted should be able to accommodate the large ohmic drop in the concretes with 'high' and 'very high' resistivities (i.e., cases of PFA and LC3). However, no guidelines are available for choosing an appropriate testing technique for highly resistive systems. Hence, many researchers tend to use the standard test methods (ASTM G109 and C876) that are suitable for the conventional S-C systems with 'low' resistivity [5,6]. The ASTM G109 specimen has three steel rebars - one rebar at the top and two rebars at the bottom (see Fig. 2(a)). During the cyclic wet-dry exposure test, the top rebar gets exposed to chlorides first and acts as anode and the bottom rebars act as cathode and the ionic conduction happens through the concrete in between. This setup enables the measurement of macrocell corrosion current between the anode and cathode in low resistive concretes (Circuit 1 in Fig. 2(b)). However, the corrosion process in highly resistive S-C systems follows Circuit 2 instead of Circuit 1 – leading to limitations in using ASTM G109 for corrosion assessment [7,8].

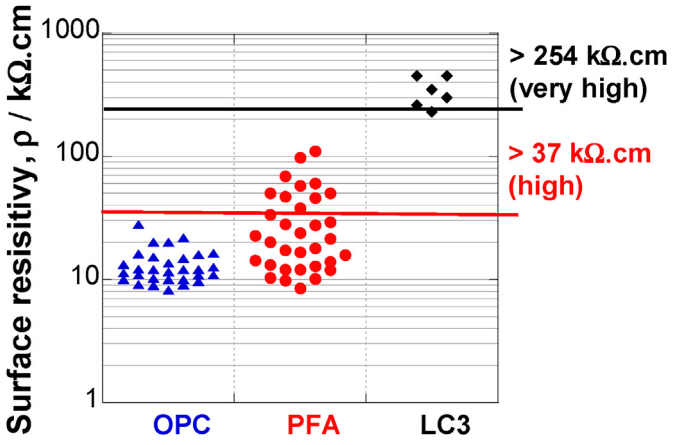

Fig. 1. Surface resistivity of concretes made with OPC, PFA, and LC3.

Table 1
AASHTO T 358 (2017) classification based on surface resistivity of concrete.

Surface Resistivity, kΩ.cm	Classification
<12	Negligible
12–21	Low
21–37	Moderate
37–254	High
>254	Very High

1.2. Factors affecting electrochemical response in S-C systems

In general, researchers have used 3-electrode systems (Working Electrode [WE], Counter Electrode [CE] and Reference Electrode [RE]) and LPR or EIS techniques to assess R_p of S-C systems [8–12]. The response data depends on various factors such as (i) electrode configuration, (ii) resistivity of electrolyte, and (iii) total current flow [13].

1.2.1. Electrode configuration

The positioning of RE in solid electrolyte is not as flexible as the liquid electrolyte [14]. Similarly, the positioning of RE in cementitious systems (a sol-gel structure with pores partially filled with liquid) is challenging. Karuppanasamy and Pillai (2017) conducted an extensive study on the Cl_{th} using a 3-electrode system with RE and an embedded Haber Luggin probe (to reach close to the embedded steel surface) [15]. A planar arrangement of electrodes (CE and WE) and Luggin probe (at pre-defined spacing of a few millimeters) all embedded in cementitious mortar was used. Authors and practicing technicians found it difficult to maintain the pre-defined spacing between the electrodes and Luggin probe while placing mortar in (say, casting) the test specimen. Also, monitoring/measuring the actual spacing/positioning of electrodes and Luggin probes in the hardened mortar was not possible. Hence, a test specimen that is easy-to-cast is necessary for obtaining reproducible results.

The current distribution across the 3-electrode cell system can be influenced by the electrode configuration, which in turn will affect the electrochemical measurements in S-C systems [16,17]. In a planar configuration, if RE is kept between CE and WE (i.e., CE-RE-WE system), then the measured solution resistance can be higher than that when the RE is kept outside CE and WE (i.e., RE-WE-CE system). Hence, the latter system is generally preferred for measuring R_p. However, Pech-Canul et al. (1998) and Zhang et al. (2014) have reported an issue with such planar arrangements for steel-cementitious and bio-anode systems, respectively [9,18]. In RE-WE-CE configuration, especially for S-C system with high resistivity, the corrosion occurring on the steel surface away from RE (i.e., between the WE and CE) may not be well-captured during the test. On the other hand, a symmetric configuration (annular geometry with CE around WE and the RE placed in between CE and WE) can accurately capture localized corrosion happening on any surface of WE [19].

The positioning of CE is also equally important. The electrochemical response from an S-C system with the CE embedded inside mortar and placed outside mortar will be different – due to significant variations in the current distribution in the two cases [9]. It was found that keeping the CE outside the mortar did not alter the response data. Also, practicing technicians would find it easy to keep CE outside the specimen than embedding inside mortar. Hence, an annular configuration with CE outside the mortar is adopted in this study. The CE surface area can also influence the electrochemical measurement and it should be chosen in such a way to avoid the rate-limiting step. To avoid this issue, ideally, the surface area of CE should be 100 times as that of the WE [20]. For practical purposes, it is recommended to use CE with at least twice the area of WE [21]. Also, literature suggests that the size (surface area) of WE should be at least 1 cm^2 [22].

1.2.2. Resistivity of electrolyte (cementitious cover)

In metal-aqueous systems, the resistivity of the electrolyte may vary significantly and nonlinearly as a function of the distance between RE and WE – the nonlinearity varies as this distance decreases [19]. This can also be attributed to the change in the pattern of equipotential lines near the WE. These factors are also applicable

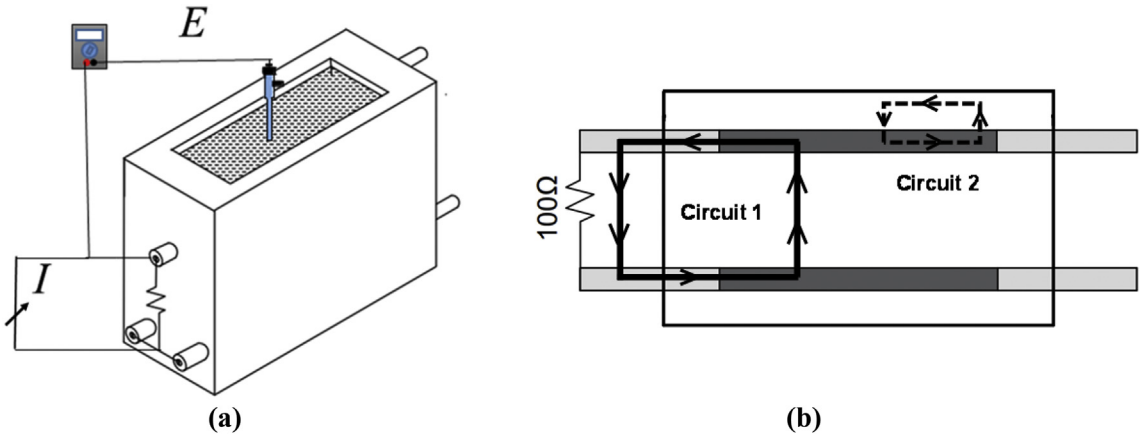

Fig. 2. ASTM G109 specimen (a) measurement of *OCP* and I_{corr} (b) different circuits.

to S-C systems and their effects on the electrochemical response from highly resistive S-C systems are not reported yet. It should be noted that the cementitious systems (sol-gel structure with pores partially filled with liquid) are poor electrolyte and resistivity at any point inside the hardened S-C systems could depend on the internal humidity, type of binder, packing density, water-binder, age, etc. There is a synergistic effect of these factors on the resistivity of the cementitious material at the S-C interface. The resistivity of the passive film formed at the surface of the steel embedded in cementitious material can also influence the electrochemical response. The pH of typical cementitious systems used in concrete structures is usually greater than 12. When steel is embedded in such alkaline cementitious systems, a thin, dense, and highly resistive passive film is formed, which prevents the underlying steel from further corrosion. The difference between the electrochemical impedance spectra of bare steel immersed in aqueous acidic system and cementitious alkaline system is not well reported in literature.

1.2.3. Input parameters for LPR measurements

To determine the R_p, the scan rate should be slow enough to fully charge the double layer capacitance (C_{dl}) of the S-C interface. Otherwise, the measured current would be a summation of current due to the corrosion reactions and charging of capacitance. The ASTM G59 recommends a scan rate of 0.1667 mVs^{-1} for metal-aqueous systems [23]. A maximum scan rate of 0.05 mVs^{-1} is recommended to measure R_p of S-C systems [24]. Researchers have used scan rates of 0.2, 0.1667, 0.1 mVs^{-1}, respectively, for measuring R_p of S-C systems [8,10,12]. The scan range also influences the measured R_p. The starting point of the scanning should be a few millivolts less than the open circuit potential (OCP) so that (i) sufficient data points are available to identify the slope of the linear region, (ii) the steel surface is not disturbed such that it becomes irreversible, and (iii) the difference between the OCP observed just before and during the sweeping is minimal. These are important while repeated tests on same specimens are involved. Scan ranges reported in literature are ±10, ±15, and ±20 mV versus OCP [8,10,12]. However, guidelines to select suitable scan rate and scan range as a function of the resistivity of S-C systems and its influence on the LPR data, especially of highly resistive S-C systems are not reported in literature.

In metal-aqueous systems, the high ohmic drop due to electrolyte is usually compensated by adopting the IR-compensation technique [25]. Successful application of this technique has been based on the consideration of Randle's circuit. The IR-compensation technique depends mainly on: (i) the duration of current interruption [on/off time], (ii) magnitude of the capacitance of the double-layer [C_{dl}], and (iii) primary and secondary current distribution between WE and RE. In S-C systems, the two major additional influencing factors are: (i) magnitude of the capacitance of the porous cementitious electrolyte and (ii) complex chemistry and moisture conditions at the S-C interface. The IR-compensation techniques have been extended successfully to S-C systems with 'low to moderate' surface resistivity (see Table 1), say less than 37 kΩ cm [8,10,12,26]. The challenges associated with the application of IR-compensation technique to highly resistive S-C systems are discussed later.

1.2.4. Input parameters for EIS measurements

The EIS technique has been successfully implemented in acquiring electrochemical response of metal-aqueous systems with high ohmic drop [27] and S-C systems with 'low to moderate' resistivity [28–30]. The AC amplitude in the range of 5–20 mV and frequency in the range of 1 MHz–1 mHz at OCP or a fixed DC potential have been used while assessing S-C systems with 'low to moderate' resistivity [30–32]. The amplitude should be chosen in such a way that a linear response is obtained while optimizing the signal-to-noise ratio [33–35]. This paper explores the feasibility and demonstrates the specifics in adopting the EIS technique to acquire and interpret the electrochemical response of highly resistive S-C systems (i.e., with significantly high ohmic drop).

2. Experimental methods

2.1. Specimen and corrosion cell test setup

Fig. 3 shows the schematic of the annular corrosion cell test setup used in this study. A lollipop type specimen with a steel reinforcement embedded at the center of a mortar cylinder was used. The cut steel pieces (8 mm diameter and 70 mm long) were cleaned by immersing in an ethanol bath in ultrasonic cleaner. The prepared steel pieces were embedded in 110 mm long cylindrical mortar (water: binder: sand ratio - 0.5:1:2.75) and ≈10 mm cover. Five lollipop specimens each were made of the following three cementitious systems: (i) OPC – 100% Ordinary Portland cement; (ii) PFA – Blend of 70% OPC and 30% PFA; and (iii) LC3 – Limestone Calcined Clay Cement.

The test specimens were cured in laboratory environment (25 ± 1 °C and 65 ± 5 %RH) for 24 ± 1 h. After this, the specimens were removed from the plastic mould and cured in fog room (25 ± 1 °C and 95 ± 3 %RH) for additional 13 days. Then, mortar surface of each specimen was coated with epoxy leaving 50 mm

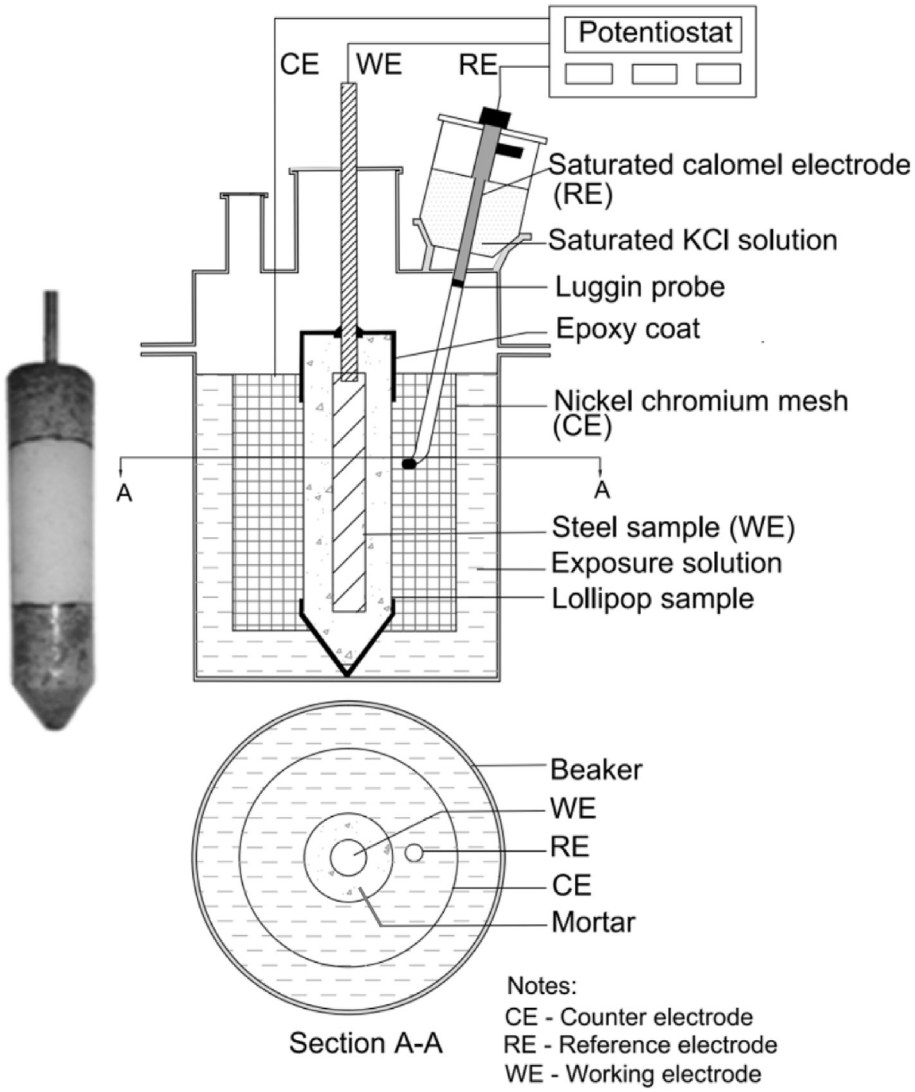

Fig. 3. Schematic of the test setup used for LPR and EIS tests.

long region in middle for exposure, as shown in Fig. 3. This was done to ensure maximum chloride ingress/attack at the middle and thereby initiating corrosion in that portion. After the epoxy was cured (say, one day), the specimens were immersed in simulated pore solution (SPS) with 3.5% NaCl until 28 days after casting. One litre of SPS is a mixture of 10.4 g of NaOH, 23.2 g of KOH and 0.3 g of $Ca(OH)_2$ in distilled water. Fig. 3 shows the schematic of the test setup used to conduct the LPR and EIS tests consisting of potentiostat, a 3-electrode corrosion cell setup with a WE, CE, and RE (embedded steel, 90 mm diameter pipe made of Nichrome wire mesh, and saturated calomel electrode [SCE], respectively). Annular arrangement with CE-RE-WE configuration was adopted. The RE was placed inside a Luggin probe, which was placed close to the surface of the mortar. The lollipop specimen was immersed in an electrolyte of SPS with 3.5% NaCl.

In metal-aqueous systems, as soon as the specimens are immersed in the electrolyte, the metal (WE) surface comes in contact with the liquid electrolyte. This is not the same in the case of steel embedded in hardened/porous S-C systems. Hence, the lollipop specimens were immersed in SPS (electrolyte) for about 48 h. Based on the unpublished results from another study in the laboratory, it was found that 2 days of immersion of the lollipop specimen in SPS ensures adequate relative humidity and oxygen conditions at the S-C interface in the specimen. Hence, all the electrochemical readings in this study were taken by connecting the corrosion cell to a potentiostat (Solartron 1287 A/1260 workstation) at the end of 2 days of immersion.

2.2. Electrochemical tests

The overall objective of the research project was to develop a Cl_{th} test for highly resistive systems [36]. For this, the chloride concentration at the S-C interface is slowly increased (by cyclic wet-dry exposure to chlorides) and accurate determination of R_p after every wet period (2 days) is needed. Corrosion initiation is defined to occur when the inverse polarization resistance ($1/R_p$) exhibits a statistically significant increase [36]. The challenge was in measuring R_p, which is addressed in the present paper by a 3-Phase experimental program.

2.2.1. Phase 1 –ability of LPR technique in detecting corrosion initiation

The objective of Phase 1 was to assess the feasibility of LPR technique in determining R_p and detecting corrosion initiation in systems with various resistivity. The lollipop specimens were subjected to cyclic wet-dry exposure (2 days wet followed by 5 days

dry) using SPS with 3.5% NaCl. After the 2-day wet period in each exposure cycle, LPR test was conducted using a scan range of ±15 mV with respect to the measured OCP and a scan rate of 0.1667 mVs^{-1}. When the R_p decreases to a value below 10 $k\Omega\,cm^2$ (say, threshold R_p) for two consecutive wet-dry cycles, testing was stopped and the specimen was autopsied for visual observation (say, presence of corrosion products). Then, the ability of LPR technique in detecting corrosion initiation was assessed by comparing it with the visual observation.

2.2.2. Phase 2 - factors affecting LPR response

Based on the observations in Phase 1, it was decided to investigate the effect of scan rate, scan range, and IR-compensation. The effect of scan rates of 0.05, 0.1, and 0.1667 mVs^{-1} and scan ranges of ±10, ±15, and ±30 mV versus OCP were investigated. Various LPR tests with IR-compensation ON was conducted. However, significant noise was observed in all the tests with IR-compensation ON. Various attempts were made to troubleshoot this; however, a suitable solution was not obtained. Hence, the suitability of EIS for determining R_p was investigated.

2.2.3. Phase 3 - factors affecting EIS response

For studying the effect of passive film on EIS response, a lollipop type steel specimen with mortar cover, as given in Fig. 3, was used. The specimen was cured for 28 days and allowed to hydrate for another four months (assuming full hydration). This ensured the formation of adequate passive film on the embedded steel surface. Then, three EIS responses were obtained as follows. First, the EIS response of the fully hydrated lollipop specimen with adequate passive film (denoted as Steel-Cementitious or S-C system, herein) was obtained. Second, the mortar cover was removed from the lollipop specimen without damaging the surface of the embedded steel rebar. Then, the steel piece was immersed in high pH SPS (denoted as Steel-Solution or S-S system, herein) and the EIS response was obtained after 2 min of immersion. Third, another EIS response was obtained from the same S-S system after 10 min of immersion.

For determining R_p using EIS, same corrosion cell setup was used. The following test parameters were studied. Based on the challenges faced during the preliminary tests, the effects of positioning of RE with respect to WE were found critical and studied. Then, the effect of two different AC perturbation signal amplitudes (±10 and ± 50 mV peak-to-peak value) were studied and an amplitude suitable for highly resistive systems was decided. Then, the electrochemical response obtained at the suitable amplitude and in a frequency range of 1 MHz to 0.01 Hz was studied and a frequency range suitable for highly resistive system was determined. In all these studies, the DC potential was maintained at OCP and data was collected at 10 points per decade.

3. Results and discussion

The ability of LPR and EIS techniques in determining the R_p of steel in OPC, PFA, and LC3 systems were assessed. These cementitious systems exhibited surface resistivities of 'low', 'moderate', and 'very high' (as per Table 1).

3.1. Phase 1 —ability of LPR technique in detecting corrosion initiation

Fig. 4 shows the inverse R_p as a function of exposure period and a typical photograph of the corroded S-C interface of the OPC, PFA, and LC3 test specimens. As shown in Fig. 4(a) and (b), the onset of corrosion was correctly detected by the electrochemical response of all the OPC and some PFA specimens. Some PFA specimens, even

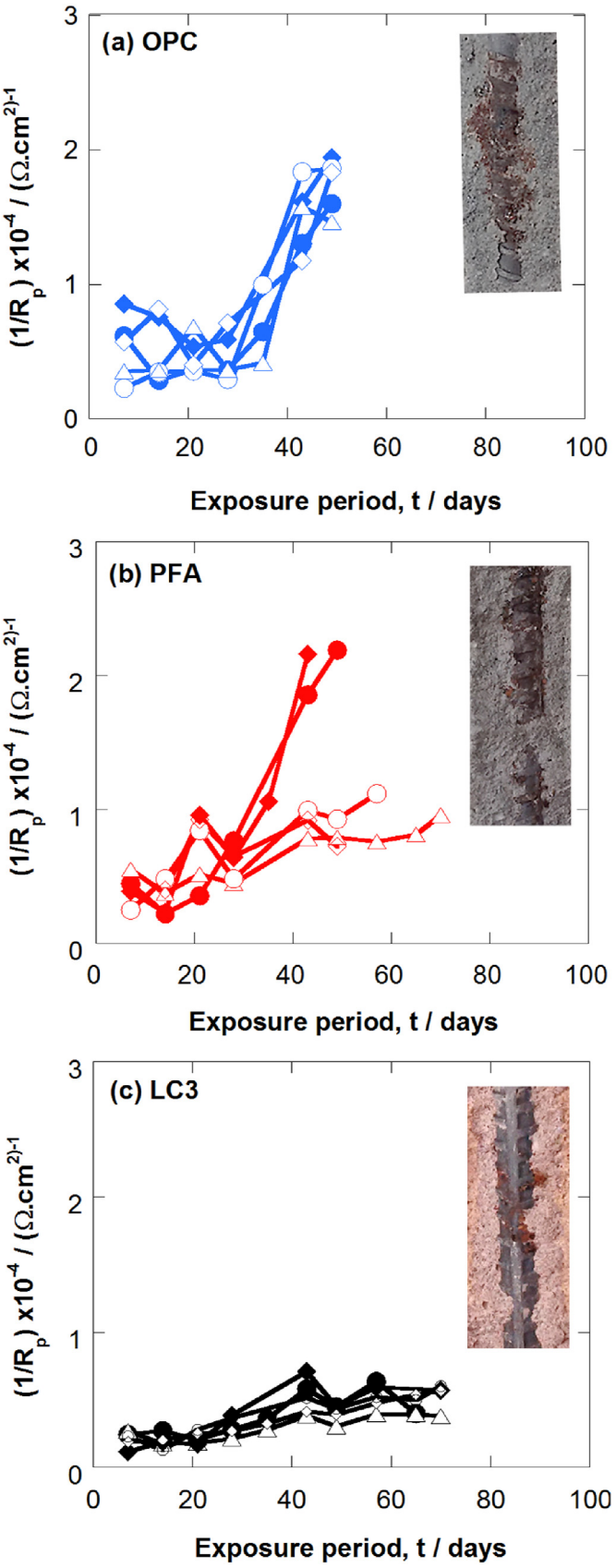

Fig. 4. Observed inverse polarization resistance of OPC, PFA and LC3 specimens on prolonged exposure to chlorides and typical visual observations.

with low $1/R_p$ exhibited corrosion stains and were found to have significant corrosion upon autopsying. This can be attributed to the significant increase in the resistivity of the mortar cover with age in those specimens. Hence, it can be concluded that the LPR technique (with adopted input parameters) is not always reliable in detecting corrosion initiation. In the case of LC3 specimens, the $1/R_p$ exhibited no significant increase until about 80 days. However, corrosion stains were observed on the surface of the mortar and visible corrosion was observed on the embedded steel surface when autopsied, as shown in Fig. 4(c). This indicates that the LPR technique was not successful in accurately determining R_p and detecting corrosion initiation of any of the LC3 systems with very high resistivity. Hence, the factors affecting the LPR response in highly resistive S-C systems were investigated.

3.2. Phase 2 - LPR response

3.2.1. Scan rate and scan range

Literature recommend a scan rate of 0.05 mVs^{-1} for LPR studies on S-C systems [24]. This particular scan rate is sufficient to charge the capacitance of double layer (C_{dl}) in S-C systems with low resistivity (say, OPC systems). Fig. 5(a) shows the effect of scan rate on electrochemical response of specimens with moderate resistivity and in passive state (negligible corrosion). It is shown that as the scan rate increases from 0.05 to 0.1667 mVs^{-1}, the R_p decreases. This is due to the increase in the current across the double layer (C_{dl}) [37]. Fig. 5(b) shows the effect of scan range on passive specimens. Increase in scan range (i.e., the difference between the starting point of scanning and original OCP) can disturb the OCP of the system resulting in higher R_p and the specimen takes longer time to return to its original OCP. Also, higher scan range may lead the response to the non-linear region; hence, the induced perturbation should be as minimum as possible. Considering this, a scan range of ±10 mV versus OCP is recommended for LPR tests in S-C systems. Although a different scan rate and scan range had been adopted in Phase 1, the effect of these parameters on $R_p$was found less than that due to the resistivity of the cementitious system (i.e., porous, sol-gel electrolyte).

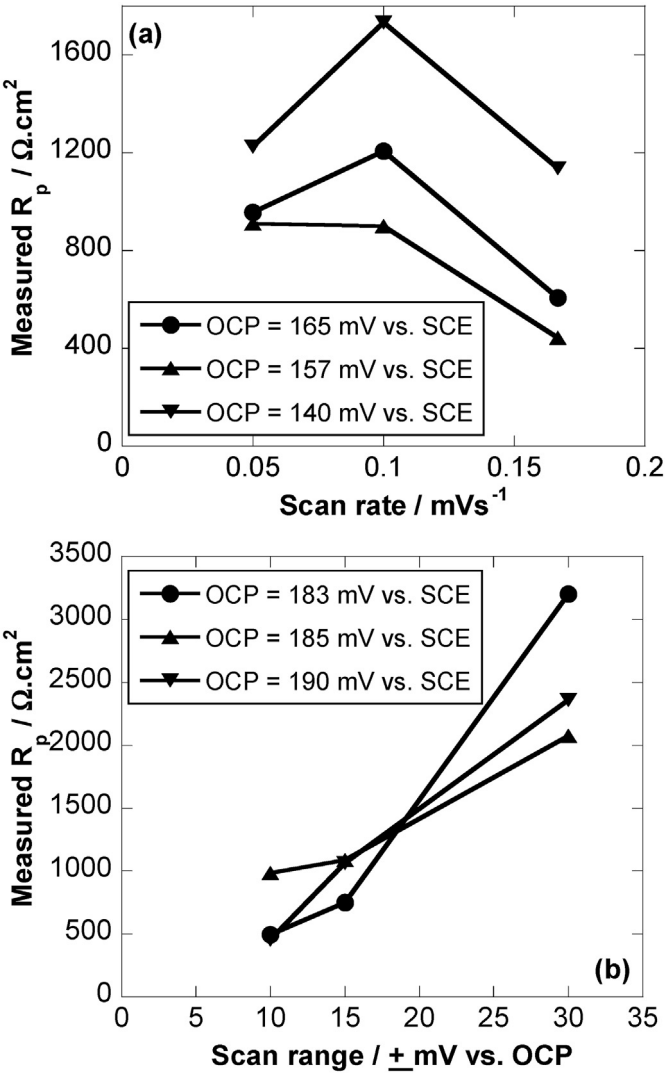

Fig. 5. Effect of (a) Scan rate and (b) Scan range on measured R_p.

3.2.2. Effect of electrolyte resistance

The LPR technique gives the combined polarization resistance exhibited by the S-C system, which includes both the resistance of mortar cover (R_m) and polarization resistance of steel (R_p). This technique has the assumption that the R_m is negligible when compared to the R_p of the specimen [38] – as in the case of a metal-aqueous system. In the case of S-C systems with highly resistive cementitious cover, the R_m is significant and comparable to R_p and hence, this assumption becomes invalid. Due to high resistivity (say, $R_m > 0.5\ R_p$), significant ohmic drop can occur in such systems [25]. Such uncompensated ohmic drop can lead to a significant distortion of the input scan rate, which in turn lead to large error in the measured R_p. When the ohmic drop is significant, LPR with positive feedback/current interrupt options is recommended to compensate the same. LPR with positive feedback involves trial and error approach, where the solution resistance measured is potential-dependent and can lead to partial compensation or overcompensation of the ohmic drop [39]. Hence, in such cases, LPR with the current interrupt method is suggested. However, this technique for highly resistive S-C systems could not be verified due to significant noise and distortion of the polarization curve. Also, the technique is based on Randle's circuit, where the electrolyte is considered to have only resistance. As cementitious system is a sol-gel structure with pores partially filled with the liquid, it has both resistance and capacitance. This might have led to noise when the instrument was set for IR-compensation. Therefore, it can be concluded that the acquisition and interpretation of reliable LPR response from highly resistive S-C systems is challenging. There is a need to understand the performance of individual components to interpret the data. Hence, the EIS technique was adopted for assessing the R_p of steel embedded in S-C systems.

3.3. Phase 3- EIS response

It was attempted to assess the R_p of the lollipop specimen using the same corrosion cell setup and EIS technique. However, a number of artefacts were observed in the Nyquist plot and are discussed in detail. Also, the effect of passive film on the EIS curve is discussed.

3.3.1. Effect of passive film

Fig. 6 (a) shows the effect of the presence of mortar cover on the EIS response from a steel specimen with passive film. The inset gives details in the high frequency region. As mentioned earlier, three EIS spectra are obtained from the (i) S-C system, (ii) S-S system with 2 min of immersion, and (iii) S-S system with 10 min of immersion. The inset provides the complete spectra of the S-C system (curve closest to the origin). The starting point of the low

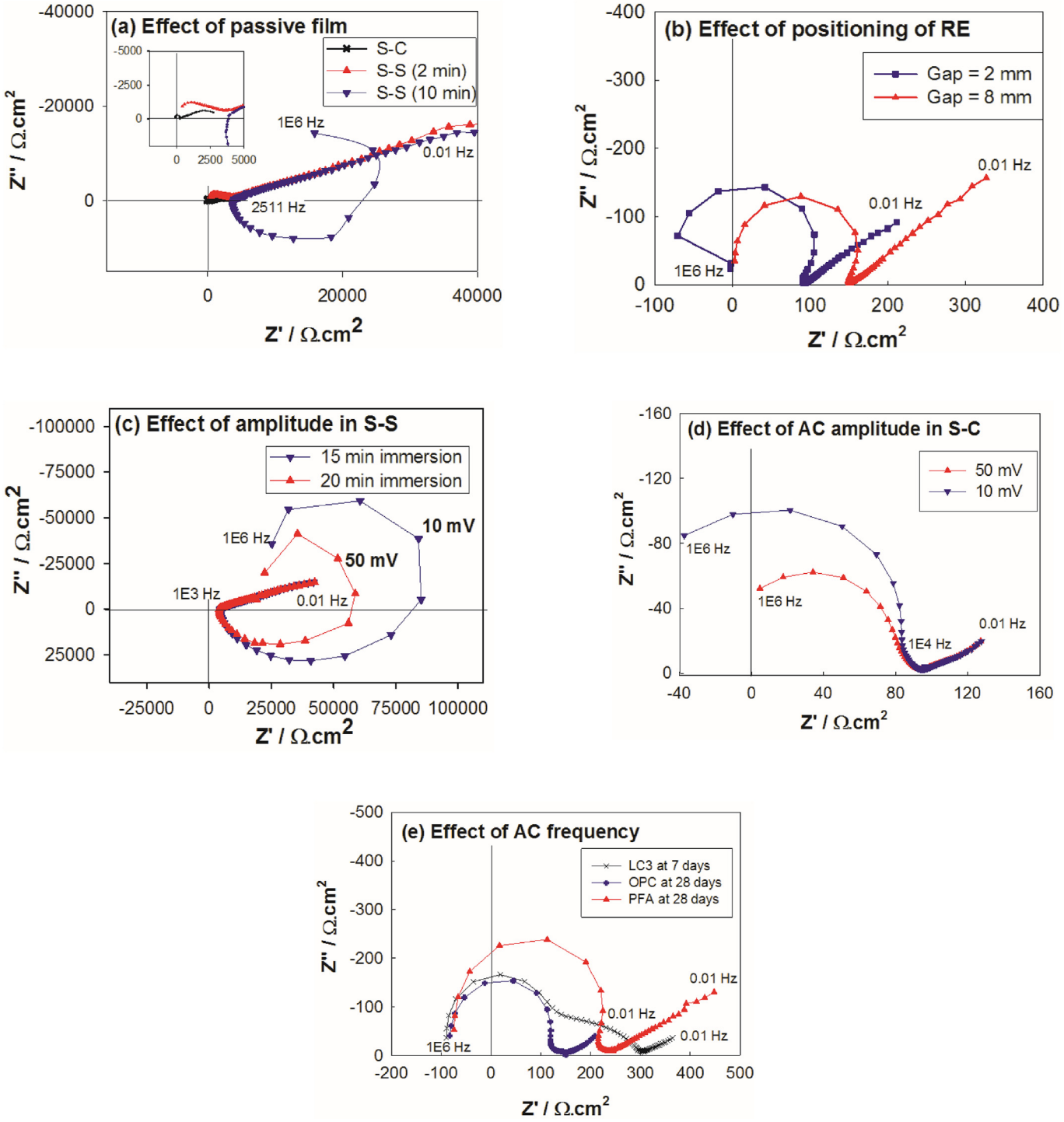

Fig. 6. Effect of various test parameters on the Nyquist plot.

frequency tail is indicative of the resistance of the mortar cover (say, about 25000Hz). The two curves of the S-S system with passive film shows difference in the high frequency region as the immersion time increases, whereas the low frequency tail coincides at about 2500 Hz, which represents the resistance of the passive film. This coincidence indicates that the resistance of the passive film is not affected by the immersion time. The deviation exhibited by the two S-S curves (near the 0.01 Hz region) is negligible.

3.3.2. Effect of the position of reference electrode (RE)

Fig. 6(a) shows the effect of the position of RE with respect to WE. When RE was kept at 2 mm away from the mortar surface of the lollipop specimen, the obtained Nyquist plot had severe distortion in the high frequency region. This could be either due to the shielding effect or short-circuiting. The shielding effect causes a redistribution of current lines as the Luggin probe physically hinders the direct current flow; whereas the close packing of current lines at the Luggin tip leads to a current cut-off and short-circuiting

due to the high impedance of the liquid in the connecting bridge (narrow tubing) of RE [40]. Shielding is an issue when the WE is very small, which is not the case in the present study. Hence, it can be concluded that the short-circuiting is the reason for the distortion in the present case. This distortion was avoided by keeping the RE at a distance of at least twice the diameter of the Luggin probe tip and inserting a platinum wire at the tip (connecting the solution inside the narrow tubing and the solution in the beaker).

3.3.3. Effect of AC amplitude and frequency range

Fig. 6 (c) and (d) shows that as the AC amplitude increases from 10 to 50 mV, the radius of the semi-circular region (in high frequency region) decreases in both S-C and S-S systems. This electrochemical shift to non-linear region is in agreement with the literature [36]. However, the low frequency tails of the EIS spectra from the S-S (about 1000 Hz) and S-C systems (about 10000 Hz) coincide and do not change with amplitude. This is due to the high resistance of the passive film against the diffusion of species from solution in S-S systems. In the case of S-C systems, this resistance is mainly offered by the highly resistive mortar surrounding the steel. This ohmic resistance is unaffected by change in amplitude [41]. Also, when the passive film is present, the instantaneous corrosion rate do not change rapidly during the EIS test. As reported in literature [36], the steel immersed in acidic solutions may not have passive film and may experience rapid change in instantaneous corrosion rate during the EIS tests, leading to a shift in the starting point of the low-frequency tail. Hence, in this study, the AC amplitude was kept at ±10 mV (peak-to-peak). Similarly, when the higher frequency range of 1 MHz was applied, a negative inductive loop in the EIS curve was observed (Fig. 6(e)). [Note: The resistivity obtained at 7th day of curing is shown for LC3 system in Fig. 6(e). The cementitious system will continue to hydrate and develop resistivity of about 2000 Ω cm^2 at 28th day of curing, which is the typical age of testing for chloride threshold.] This could be due to noise picked up by the cables, which in turn leads to distortion (shift of the Nyquist plot in the negative quadrant of Z') in the high-frequency region [42] or due to the high impedance of the liquid inside the narrow tubing of the luggin probe. The response time of RE, especially in the high frequency is severely affected by such high impedance [43]. As the luggin probe was designed with a platinum wire inserted at the tip, this effect could be mainly due to the noise picked up by the cables. To mitigate this artefact, the maximum frequency was reduced from 10^6 to 10^5 Hz, which is still sufficient to capture the electrochemical response in S-C systems. The high frequency distortion is independent of the type of cement or binder being used. Hence, these precautions for positioning and input parameters should be taken to get good electrochemical response from highly resistive S-C systems.

3.3.4. EIS curve

The specimens were tested using EIS by over siding a perturbation signal of ±10 mV (peak-to-peak) amplitude at OCP and by sweeping the frequency from 10^5 to 0.01 Hz. The data was collected at 10 points per decade. Fig. 7 shows the typical Nyquist plots in OPC, PFA1 (low resistivity), PFA2 (moderate resistivity), and LC3 specimens. For better clarity, the Nyquist plots in OPC, PFA1 and PFA2 specimens are shown separately as an inset in Fig. 7. There is a huge variation in the measured R_m in these systems due to their resistivity. This remarkable difference in resistivity, especially in LC3 could have led to a distortion of the electrochemical response from LPR tests. The summation of high resistance from cover (R_m) and the polarization resistance of steel (R_p) in LC3 systems results in high measured values for combined ($R_m + R_p$) response, irrespective of ongoing corrosion. Note that LPR technique cannot differentiate the R_p and R_m from the combined ($R_m + R_p$) response.

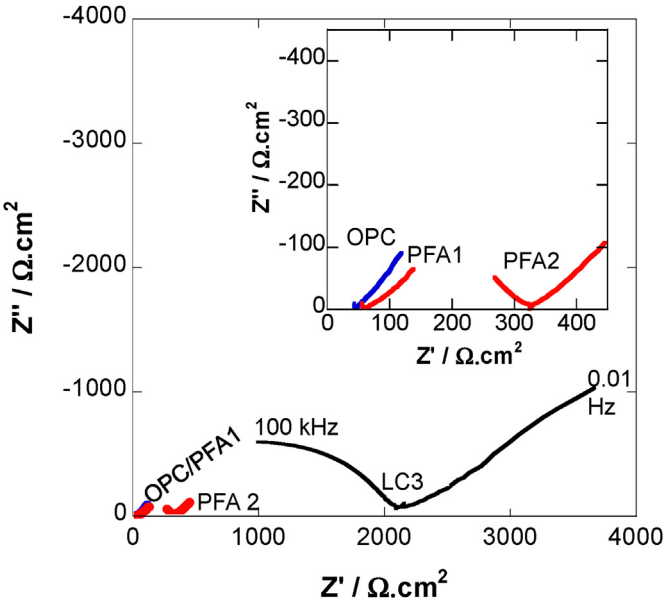

Fig. 7. Typical Nyquist plot of OPC, PFA and LC3 specimens.

Because of these, the reduction in R_p due to the initiation of corrosion could not be detected adequately. In the case of EIS technique, the contribution of resistance from each component can be obtained with the help of a suitable equivalent circuit and fitting – helps in separately monitoring the reduction in R_p and detecting corrosion initiation. Another advantage of EIS technique is that the correctness of the electrochemical response can be verified using Kramer-Kraig Transform (KKT). Once verified with KKT, the R_p can be obtained by extracting the value from the equivalent electrical circuit fit.

3.3.5. Equivalent electrical circuit

The frequency spectra obtained from PFA and LC3 systems deviate from the conventional spectra revealing a diffusion process (negative slope of the 45° phase - conforming to Warburg type elements) obtained in OPC systems. This is mainly due to the difference in the geometry of the pore structure and tortuosity between these systems [44]. The PFA and LC3 systems have very small refined pores, which lead to greater tortuosity than the OPC systems with straight and bigger open pores [45]. Since there is a deviation in the low-frequency region from 45°, conventional Randles circuit cannot be used to model the equivalent circuit for highly resistive S-C systems. In this study, the response from all the S-C systems is modelled as a porous electrode, as shown in Fig. 8(a), irrespective of the difference in resistivity in the specimens. In Fig. 8(a), the resistance (R_m) and constant phase element-CPE (C_m) represent the mortar cover, the $R_{interface}$ and C_{dl} (non-ideal capacitive nature of double layer represented as CPE) represent the S-C interface, and the R_p and C_{pf} represent the porous electrode (Non ideal passive film on the steel surface, represented as CPE). With the circuit analysis, keeping the chi-squared value less than 0.001 and error of the individual components less than 20%, the R_p of steel can be obtained separately. Typical response and fit of EIS data from steel embedded in LC3 system are shown in Fig. 8(b) and (c).

3.3.6. Detection of corrosion initiation

Determination of Cl_{th} is essential for the estimation of service life, for which repeated measurements of R_p of steel embedded in hardened cementitious system are required until the corrosion initiation criteria is met. Fig. 9(a) shows the difference in R_p

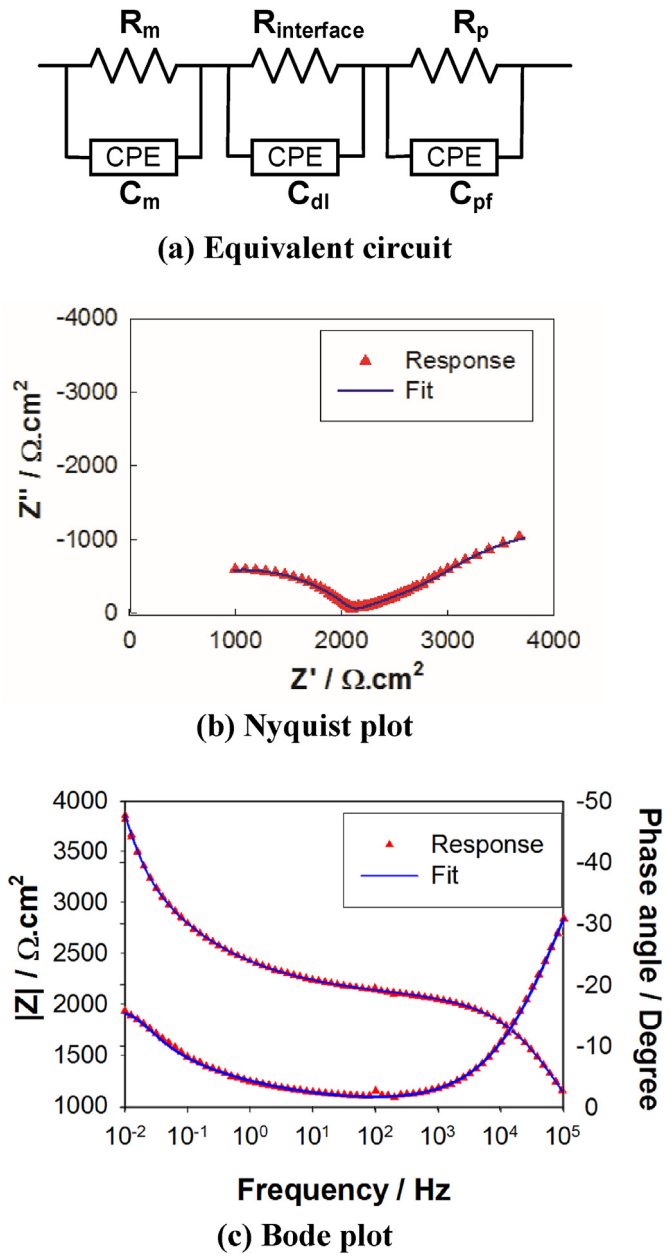

Fig. 8. Chosen equivalent circuit and typical circuit fits in LC3.

obtained from LPR and EIS in a typical LC3 specimen. In this study, a statistically based initiation criteria [15] was adopted. In LC3 systems, due to the high R_m, the LPR technique could not detect the corrosion as soon as it was initiated. The earlier corrosion initiation was justified with the observation of a deep pit, which would take several days to form, under the given experimental conditions. Fig. 9(b) and (c) show the photograph and tomographic image of the corrosion pit observed when autopsied. The analysis of the pit dimensions indicated a cross sectional loss of about 4% at that section of the rebar. This kind of deep pit cannot form in a single exposure cycle indicating that the LPR data could not detect the ongoing corrosion as soon as it was initiated. The LPR technique can detect corrosion only when the resistivity of the mortar cover is low. Table 2 gives the number of testing cycles taken to detect the corrosion initiation when LPR and EIS techniques were used. The EIS technique detects corrosion at early stages itself, which is not the case with LPR. LPR technique is able to detect corrosion only at later stages when the R_m reduces to 'low' value (see Table 1), probably due to the significant increase in chloride concentration. Thus, in highly resistive cementitious systems (say, $\rho > 37\ k\Omega\ cm$), for the adopted test parameters and cell geometry, the EIS technique suits better for early detection of corrosion initiation.

4. Conclusions

The following conclusions were made based on the experimental work.

1. Linear polarization resistance (LPR) technique without current interruption/positive feedback did not show any indication of ongoing corrosion in highly resistive concrete systems (surface resistivity, $\rho > 37\ k\Omega\ cm$) when the resistance of mortar cover (R_m) is comparable to the polarization resistance of steel (R_p). Also, acquiring a good LPR curve using the current interruption technique was challenging in the adopted electrode configuration.

Table 2
Testing cycles - LPR vs. EIS.

Specimen Number	Number of cycles to detect corrosion initiation		
	LPR	EIS	Difference
S1	17	7	10
S2	12	9	3
S3	15	8	7
S4	14	7	7

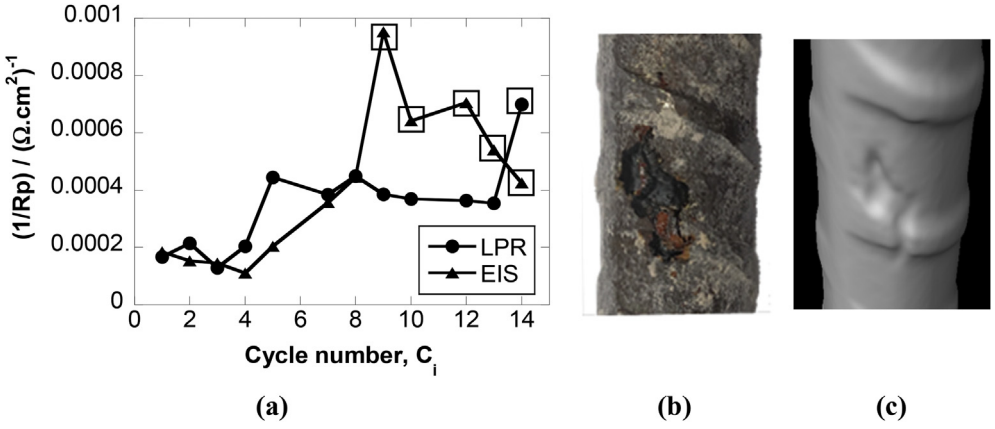

Fig. 9. (a) Electrochemical response from EIS and LPR techniques (b) photograph showing deep pit and (c) tomographic image showing deep pit.

2. For LPR tests on steel-cementitious (S-C) systems, a scan rate of 0.05 mVs^{-1} and a scan range of ±10 mV versus OCP are recommended.
3. In EIS spectra of S-C systems with passive film on the steel surface and highly resistive mortar surrounding the steel, the ohmic resistance and the starting point of the low-frequency tail is unaffected by change in amplitude.
4. For EIS tests on S-C systems, an AC amplitude of ±10 mV (peak-to-peak) and a frequency of 10^5 to 0.01 Hz at OCP are recommended.
5. A minimum spacing of twice the diameter of the tip of luggin probe must be maintained and the ohmic drop at the tip of the luggin probe must be low to avoid artefacts in EIS response from S-C systems, irrespective of the resistivity.
6. Randles circuit is not suitable for steel embedded in highly resistive concrete systems. Suitable equivalent circuit should be chosen according to the S-C systems under study.
7. EIS with the studied electrode configuration and selected input parameters can be used for monitoring changes in the R_p of steel embedded in highly resistive cementitious systems and detecting corrosion initiation at early stages.

Acknowledgements

The authors acknowledge the financial support from Department of Science and Technology (DST), Government of India (SERB Sanction No EMR/2016/003196). Also, the financial support from the Ministry of Human Resources Development, Government of India, and the Department of Civil Engineering, Indian Institute of Technology Madras, Chennai is acknowledged. The assistance from Prof. Ravindra Gettu, Prof. Manu Santhanam and Prof. S. Ramanathan, and the laboratory staff and students in the Construction Materials Research Laboratory at IIT Madras is also appreciated.

References

[1] K.L. Scrivener, 202 special issue - options for the future of cement, Indian Concr. J. 88 (2014) 11–21, https://doi.org/10.1002/(SICI)1097-0045(19990501)39:2<108::AID-PROS5>3.0.CO; 2-9.
[2] Y. Dhandapani, T. Sakthivel, M. Santhanam, R. Gettu, R.G. Pillai, Mechanical properties and durability performance of concretes with limestone calcined clay cement (LC3), Cement Concr. Res. 107 (2018) 136–151, https://doi.org/10.1016/j.cemconres.2018.02.005.
[3] B.S. Dhanya, Study of the Influence of Supplementary Cementitious Materials on Selected Durability Parameters of Concrete, PhD Thesis, Indian Institute of Technology Madras, Chennai, India, 2015.
[4] AASHTO T 358, Standard Method of Test for Surface Resistivity Indication of Concrete's Ability to Resist Chloride Ion Penetration, American Association of State Highway and Transportation Officials, Washington, D.C., U.S.A., 2017.
[5] ASTM G 109, Standard Test Method for Determining Effects of Chemical Admixtures on Corrosion of Embedded Steel Reinforcement in Concrete Exposed to Chlorides, ASTM Stand., 2005, pp. 1–6, https://doi.org/10.1520/G0109-07.2.
[6] ASTM C 876, Standard Test Method for Half-Cell Potentials of Uncoated Reinforcing Steel in Concrete, vol. 91, 1999, pp. 1–6, https://doi.org/10.1520/C0876-09.2.
[7] S. Rengaraju, A. Godara, P. Alapati, R.G. Pillai, Macrocell corrosion mechanisms of prestressing strands in various concretes, Mag. Concr. Res. 109 (2018) 1–13.
[8] C.M. Hansson, A. Poursaee, A. Laurent, Macrocell and microcell corrosion of steel in ordinary Portland cement and high performance concretes, Cement Concr. Res. 36 (2006) 2098–2102, https://doi.org/10.1016/j.cemconres.2006.07.005.
[9] C. Andrade, C. Alonso, Corrosion rate monitoring and on-site, Constr. Build. Mater. Elsevier. 10 (1996) 315–328.
[10] A.A. Pech-Canul, M.A. Sagüés, P. Castro, Influence of counter electrode positioning on solution resistance in impedance measurements of reinforced concrete, Corrosion 54 (1998) 663–667.
[11] D. Trejo, R.G. Pillai, Accelerated chloride threshold Testing : Part I — ASTM a 615 and A 706 reinforcement, ACI Mater. J. (2003) 519–527.
[12] U.M. Angst, B. Elsener, C.K. Larsen, Ø. Vennesland, Chloride induced reinforcement corrosion: electrochemical monitoring of initiation stage and chloride threshold values, Corros. Sci. 53 (2011) 1451–1464, https://doi.org/10.1016/j.corsci.2011.01.025.
[13] H.P. Hack, P.J. Moran, J.R. Scully, Influence of electrolyte resistance on electrochemical measurements and procedures to minimize or compensate for resistance errors, in: L.L. Scribner, S.R. Talylor (Eds.), The Measurement and Correction of Electrolyte Resistance in Electrochemical Tests, ASTM, Philadephia, 1990, pp. 5–26. STP1056.
[14] J. Rutman, I. Riess, Placement of reference electrode in solid state electrolyte cells, Solid State Ionics 179 (2008) 913–918, https://doi.org/10.1016/j.ssi.2008.01.071.
[15] J. Karuppanasamy, R.G. Pillai, A short-term test method to determine the chloride threshold of steel–cementitious systems with corrosion inhibiting admixtures, Mater. Struct. Constr. 50 (2017) 1–17, https://doi.org/10.1617/s11527-017-1071-1.
[16] C. Andrade, L. Soler, C. Alonso, X.R. Nbvoa, M. Keddamt, The importance of geometrical consideration in the measurement of steel corrosion in concrete by means of AC impedance, Pergamon Corros. Sci. 37 (1995) 2013–2023, https://doi.org/10.1016/0010-938X(95)00095-2.
[17] J.C. Myland, K.B. Oldham, Uncompensated resistance. 1. The effect of cell geometry, Anal. Chem. 72 (2000) 3972–3980, https://doi.org/10.1021/ac0001535.
[18] F. Zhang, J. Liu, I. Ivanov, M.C. Hatzell, W. Yang, Y. Ahn, et al., Reference and counter electrode positions affect electrochemical characterization of bioanodes in different bioelectrochemical systems, Biotechnol. Bioeng. 111 (2014) 1931–1939, https://doi.org/10.1002/bit.25253.
[19] G. Hsieh, T.O. Mason, E.J. Garboczi, L.R. Pederson, Experimental limitations in impedance spectroscopy: Part III. Effect of reference electrode geometry/position, Solid State Ionics 96 (1997) 153–172, https://doi.org/10.1016/S0167-2738(97)00075-1.
[20] JohnO.M. Bockris, A.K.N. Reddy, M.E. Gamboa-Aldeco, Modern Electrochemistry 2A Fundamentals of Electrodics, second ed., Kluwer Academic Publishers, New York, 2000.
[21] ASTM G61-86 (Reapproved 2014), Standard test method for conducting cyclic potentiodynamic polarization measurements for localised corrosion susceptibility of Iron-,Nickel-,or cobalt-based alloys 86 (2014) 1–9, https://doi.org/10.1520/F2129-08.Copyright.ASTM (2014) G61-86.
[22] ASTM G5 Standard Reference Test Method for Making Potentiodynamic Anodic Polarization Measurements, 2014, pp. 1–8, https://doi.org/10.1520/G0005-13E02.2.
[23] ASTM G59-97, Standard test method for conducting potentiodynamic polarization resistance measurements, ASTM Int 97 (2014) 1–4, https://doi.org/10.1520/G0059-97R14.2.
[24] A. Poursaee, Determining the appropriate scan rate to perform cyclic polarization test on the steel bars in concrete, Electrochim. Acta 55 (2010) 1200–1206, https://doi.org/10.1016/j.electacta.2009.10.004.
[25] F. Mansfeld, The effect of uncompensated IR-drop on polarization resistance measurements, Corrosion 32 (1976).
[26] A.A. Sagues, S.C. Kranc, On the determination of polarization diagrams of reinforcing steel in concrete, Corrosion 48 (1992) 624–633, https://doi.org/10.5006/1.3315982.
[27] N. Perini, A.R. Prado, C.M.S. Sad, E.V.R. Castro, M.B.J.G. Freitas, Electrochemical impedance spectroscopy for in situ petroleum analysis and water-in-oil emulsion characterization, Fuel 91 (2012) 224–228, https://doi.org/10.1016/j.fuel.2011.06.057.
[28] V. Feliu, J.A. González, C. Andrade, S. Feliu, Equivalent circuit for modelling the steel-concrete interface. II. Complications in applying the Stern-Geary equation to corrosion rate determinations, Corros. Sci. 40 (1998) 995–1006, https://doi.org/10.1016/S0010-938X(98)00037-7.
[29] A.A. Sagüés, M.A. Pech-Canul, A.K.M. Shahid Al-Mansur, Corrosion macrocell behavior of reinforcing steel in partially submerged concrete columns, Corros. Sci. 45 (2003) 7–32, https://doi.org/10.1016/S0010-938X(02)00087-2.
[30] D.V. Ribeiro, J.C.C. Abrantes, Application of electrochemical impedance spectroscopy (EIS) to monitor the corrosion of reinforced concrete: a new approach, Constr. Build. Mater. 111 (2016) 98–104, https://doi.org/10.1016/j.conbuildmat.2016.02.047.
[31] R.G. Duarte, A.S. Castela, R. Neves, L. Freire, M.F. Montemor, Corrosion behavior of stainless steel rebars embedded in concrete: an electrochemical impedance spectroscopy study, Electrochim. Acta 124 (2014) 218–224, https://doi.org/10.1016/j.electacta.2013.11.154.
[32] O. Poupard, A. Aït-Mokhtar, P. Dumargue, Corrosion by chlorides in reinforced concrete: determination of chloride concentration threshold by impedance spectroscopy, Cement Concr. Res. 34 (2004) 991–1000, https://doi.org/10.1016/j.cemconres.2003.11.009.
[33] K. Darowicki, The amplitude analysis of impedance spectra, Electrochim. Acta 40 (4) (1995) 439–445.
[34] B. Hirschorn, B. Tribollet, M.E. Orazem, On selection of the perturbation amplitude required to avoid nonlinear effects in impedance measurements, Isr. J. Chem. 48 (2008) 133–142, https://doi.org/10.1560/IJC.48.3-4.133.
[35] S.N. Victoria, S. Ramanathan, Effect of potential drifts and ac amplitude on the electrochemical impedance spectra, Electrochim. Acta 56 (2011) 2606–2615, https://doi.org/10.1016/j.electacta.2010.12.007.
[36] S. Rengaraju and R.G. Pillai, Determination of Chloride Threshold in Limestone Calcined Clay Cement, (Unpublished results).
[37] M.A. Ameer, E. Khamis, M. Al-Motlaq, Electrochemical behaviour of recasting Ni-Cr and Co-Cr non-precious dental alloys, Corros. Sci. 46 (2004) 2825–2836, https://doi.org/10.1016/j.corsci.2004.03.011.
[38] M.G. Fontana, Corrosion Engineering, third ed., McGraw-Hill, Singapore, 1987.
[39] F. Mansfeld, Effect of uncompensated resistance on the true scan rate in

potentiodynamic experiments, Corrosion 38 (1982) 556–559.
[40] K.B. Oldham, N.P.C. Stevens, Uncompensated resistance. 2. The effect of reference electrode nonideality, Anal. Chem. 72 (2000) 3981–3988, https://doi.org/10.1021/ac000154x.
[41] D. Szymczewska, J. Karczewski, A. Chrzan, P. Jasiński, Three electrode configuration measurements of electrolyte-diffusion barrier cathode interface, J. Ceram. Soc. Jpn. 123 (4) (2015) 268–273.
[42] H. Göhr, M. Mirnik, C.A. Schiller, Distortions of high frequency electrode impedance, J. Electroanal. Chem. Interfacial Electrochem. 180 (1984) 273–285, https://doi.org/10.1016/0368-1874(84)83586-8.
[43] W. Botter, D.M. Scares, O. Teschke, The influence of the Luggin capillary on the response time of a reference electrode, J. Electroanal. Chem. 267 (1989) 279–286, https://doi.org/10.1016/0022-0728(89)80255-4.
[44] S.J. Cooper, A. Bertei, D.P. Finegan, N.P. Brandon, Simulated impedance of diffusion in porous media, Electrochim. Acta 251 (2017) 681–689, https://doi.org/10.1016/j.electacta.2017.07.152.
[45] Y. Dhandapani, M. Santhanam, Assessment of pore structure evolution in the limestone calcined clay cementitious system and its implications for performance, Cement Concr. Compos. 84 (2017) 36–47, https://doi.org/10.1016/j.cemconcomp.2017.08.012.